Indoor Pedestrian Navigation Research
Based on Zero Velocity Correction and Sliding Window

Boqi Wu, Chenyang Cao,Yang Zhao, and Yaodan Chi[*]

Jilin Jianzhu University, No. 5088 Xincheng Street, Changchun City, Jilin 130118, China

The accuracy requirements for indoor pedestrian navigation are steadily increasing. Traditional algorithms in inertial navigation systems face issues such as cumulative errors and unclear heading research, significantly impeding the application and development of inertial navigation. In response to the accumulation of errors in traditional strap-down algorithms, we propose a gait detection method based on the generalized likelihood ratio test to more effectively identify footstep stationary states. By combining Kalman filtering with sliding window, the zero velocity correction method corrects the cumulative error issue in the inertial measurement unit of the inertial system, thus addressing the problem of low pedestrian walking accuracy in navigation. Experimental results indicate that the zero velocity correction and sliding window approach can reduce endpoint positioning errors to less than 2%, providing accurate and continuous positioning information.

1.   Introduction

With the development of portable sensing technology, applications of and research on pedestrian navigation and positioning technologies have been significantly promoted. Currently, navigation and positioning technologies predominantly rely on global navigation satellite systems (GNSSs).[1–3] However, in indoor environments, GNSS technology is hindered owing to weak satellite signals.

Current indoor navigation technologies can be broadly categorized into three classes: cross-processing technologies based on wireless communication signals,[4–7] map-matching technologies based on databases, and Micro-Electro-Mechanical System (MEMS) inertial sensor navigation technologies. Cross-processing technologies based on wireless communication signals primarily include Bluetooth, ZigBee, and ultra-wideband (UWB) positioning technologies. These systems establish multiple wireless network nodes to locate pedestrians. Among these, UWB systems offer high positioning accuracy, low power consumption, and strong penetration capabilities.[8–10] However, they require high clock synchronization precision and have high costs, hindering widespread application and adoption. Database-based WiFi

---

positioning and simultaneous localization and mapping technologies have the drawback of requiring the creation and maintenance of related databases.[11–13]

On the other hand, MEMS inertial sensors are small in size, low in power consumption, cost-effective, and easily digitized. They find wide applications in navigation and positioning with stringent hardware cost and size requirements. They utilize an inertial measurement unit (IMU) to measure the acceleration and angular velocity of aircraft or vehicles and calculate navigation parameters such as position, velocity, and attitude using motion equations. Inertial navigation systems are widely used in aerospace, defense, marine, transportation, industrial, and other fields owing to their high precision, rapid response, and strong independence. In recent years, with the development of MEMS technology and cost reduction, inertial navigation systems have made further progress.

At present, inertial navigation systems can be classified into two categories. First, there is pedestrian dead reckoning (PDR),[14–16] which uses inertial sensors such as accelerometers and gyroscopes to measure the acceleration and angular velocity of human movement. It is employed to detect step length and walking direction, using an accumulation method to calculate human position, attitude, and movement trajectory. However, factors such as walking speed and terrain have a significant impact on the accuracy and stability of PDR technology, and errors accumulate over time. Second, a strap-down inertial navigation system (SINS) is a positioning and navigation technology based on an IMU.[17] Its fundamental principle is to measure the object's acceleration and angular velocity using inertial sensors and then calculate object position, velocity, and attitude based on a dynamic model and state estimation algorithm. Compared with PDR technology, SINS offers higher accuracy and independence, enabling precise positioning and navigation in various environments and conditions.

To achieve further improvement of navigation and positioning performance, scholars at home and abroad have tried to combine other external sensors with foot micro-inertial sensors. Bebek *et al.* investigated a navigation shoe system combining a low-precision micro IMU (MIMU) with a ground reaction force sensor, which narrowed down the positioning solution error of pedestrians within half an hour's walking to about 4 m.[5] Tian *et al.* investigated a zero-speed interval detection method using an inertial sensor and a pressure sensor for zero-speed interval detection, which improved the zero-speed correction by increasing the accuracy of zero-speed interval detection. In addition to the above research line of combining with external sensors, the combination of multiple MIMUs is also a hot topic.[7] Skog *et al.* proposed an optimization method for inertial pedestrian navigation by setting up MIMUs in both feet separately and using the distance between the feet to establish inequality constraints to assist the zero-speed correction.[9] Li *et al.* proposed a single-footed dual-MIMU design, in which the dual MIMUs are placed at the tip and root of a single foot, utilizing the distance between their feet to create an unequal constraint.[14] The design of a single-legged dual MIMU is based on the idea of equational constrained Kalman filtering by utilizing the constant value of the distance between the tip and root of the single-legged MIMU, and an improved scheme is designed on the basis of the idea of equational constrained Kalman filtering. Shi *et al.*[11] investigated a bipedal dual-MIMU navigation error correction method using the unequal relationship to establish the constrained Kalman filter and constructed a ball constraint model based on the positional

relationship of the biped and maximum step size limitation. After combining devices such as pressure sensors, the accuracy of MIMU-based pedestrian navigation is effectively improved.[11] However, the addition of external components such as pressure sensors increases the complexity of the pedestrian navigation system, which is not conducive to the popularization of the system's application.

By reading and summarizing the findings in the literature, we found that the single technology's own limitations are difficult to avoid, and the combined system research has become the trend in the field of indoor navigation. Inertial navigation is often used as the main system in the construction of the combined system, and the problem of cumulative errors in inertial guidance systems is still a hot research issue to be resolved. In addition, in recent years, the combination method based on inertial guidance and UWB has received wide attention, and a method to construct a low-cost and high-efficiency combination system and realize data fusion is still being searched. In this study, we adopted the strap-down inertial navigation technology, introduced the use of the generalized likelihood ratio test (GLRT) for zero velocity detection,[6] and employed a combination of the sliding window algorithm and Kalman filtering for zero velocity correction, thus achieving a more accurate pedestrian path.

2. Design

Taking into consideration various factors such as weight, volume, sensitivity, cost, and sampling rate, we chose using BWT901BLECL5.0, an integrated high-precision three-axis gyroscope, and an accelerometer inertial sensor suite. This system involves attaching the IMU to the pedestrian's foot to collect acceleration and angular velocity data related to the pedestrian's foot movement. By applying strap-down inertial navigation algorithms, the system calculates the pedestrian's posture and position, enabling precise pedestrian localization and navigation.

However, traditional strap-down inertial navigation algorithms suffer from decreasing accuracy as the distance between the sensor and the reference point increases, rendering the results unusable. To address this issue, we focused on three key research areas. As illustrated in Fig. 1, the first aspect involves employing zero velocity correction algorithms to resolve cumulative errors in pure inertial navigation calculations, thus achieving basic functionality. The
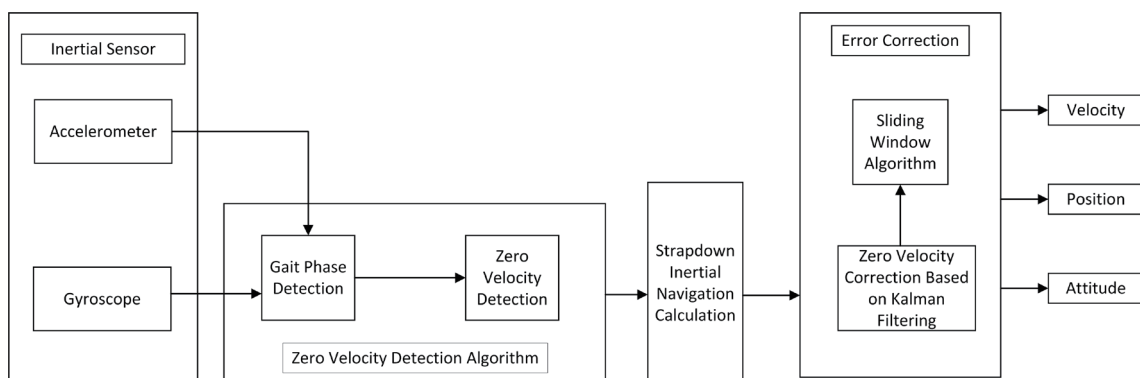
Fig. 1.   Design process flow.

second aspect introduces the use of a sliding window algorithm for pedestrian gait analysis. Data is divided into multiple consecutive windows, with data processing and feature extraction occurring within each window. In each window, statistics such as the average and variance of acceleration and angular velocity data collected by the inertial sensors are computed to derive gait characteristics for that period. This approach enhances real-time gait recognition and responsiveness. The third aspect involves the utilization of Kalman filtering to assess system errors and further correct navigation errors, thereby enhancing navigation accuracy. By reducing reliance on external devices in practical applications, the system gains greater reliability and robustness. This approach offers broad potential applications in the field.

3. Basic Information Processing

3.1 Coordinate transformation

Coordinate transformation is a crucial aspect of information exchange between navigation and the IMU. It involves the conversion of the carrier coordinate system to the navigation coordinate system, enabling the analysis and assessment of the carrier's state. In the spatial context, there are two primary coordinate systems: the navigation coordinate system (N-frame) and the carrier coordinate system (B-frame).

A commonly used navigation coordinate system (N-frame) is the "East-North-Up" geodetic coordinate system, which is a right-handed Cartesian coordinate system. In this coordinate system, the X_n-, Y_n-, and Z_n-axes point to the east, north, and zenith directions of Earth, respectively. The carrier coordinate system (B-frame) is fixed in relation to the IMU and changes with the motion of the carrier. It is defined with the X_b-axis pointing forward, the Y_b-axis pointing to the left, and the Z_b-axis formed according to the right-hand rule concerning the X_b- and Y_b-axes. The origin is positioned at the center of gravity of the IMU. The initial values of the gyroscope and accelerometer are relative to the carrier coordinate system and are determined through the static calibration of the IMU.

The transformation of the coordinate system from the carrier coordinate system (B-frame) to the navigation coordinate system (N-frame) is achieved through three consecutive rotations about different coordinate axes, as described below: rotation about the Z_b-axis of the navigation coordinate system by an angle γ, rotation about the X_n-axis of the carrier coordinate system by an angle β, and rotation about the Y_n-axis of the carrier coordinate system by an angle α.

The transformation process is illustrated in Fig. 2. The transformation matrices for each of these individual rotations are denoted as C_α, C_β, and C_γ.

$$C_\alpha = \begin{pmatrix} \cos\alpha & 0 & \sin\alpha \\ 0 & 1 & 0 \\ -\sin\alpha & 0 & \cos\alpha \end{pmatrix}, C_\beta = \begin{pmatrix} 1 & 0 & 0 \\ 0 & \cos\beta & -\sin\beta \\ 0 & \sin\beta & \cos\beta \end{pmatrix}, C_\gamma = \begin{pmatrix} \cos\gamma & -\sin\gamma & 0 \\ \sin\gamma & \cos\gamma & 0 \\ 0 & 0 & 1 \end{pmatrix}. \tag{1}$$
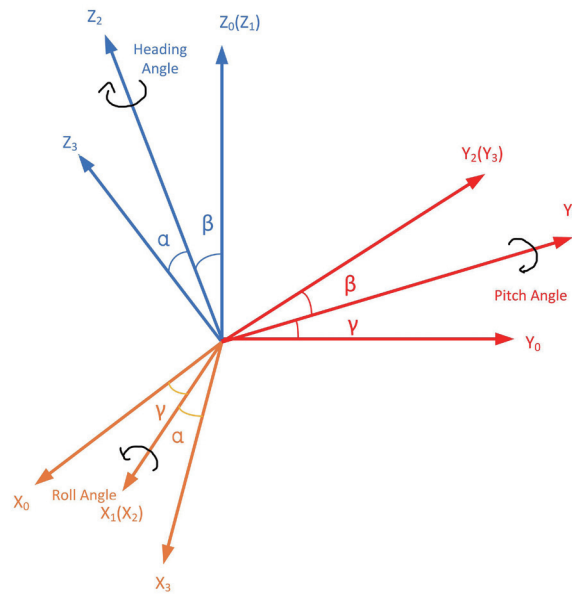
Fig. 2.   (Color online) Attitude change schematic.

The transformation matrix C_b^n for the conversion from the carrier coordinate system (B-frame) to the navigation coordinate system (N-frame), based on the order of rotations in three-dimensional space, is

$$C_b^n = C_\gamma C_\beta C_\alpha, \tag{2}$$

$$C_b^n = \begin{pmatrix} \cos\gamma\cos\alpha - \sin\gamma\sin\beta\sin\alpha & -\sin\gamma\cos\beta & \cos\gamma\sin\alpha + \sin\gamma\sin\beta\cos\alpha \\ \sin\gamma\cos\alpha + \cos\gamma\sin\beta\sin\alpha & \cos\gamma\cos\beta & \sin\gamma\sin\alpha - \cos\gamma\sin\beta\cos\alpha \\ -\cos\beta\sin\alpha & \sin\beta & \cos\beta\cos\alpha \end{pmatrix}. \tag{3}$$

In describing attitude changes, quaternions are employed. Quaternions are recognized as a vector with four components, denoted as q, comprising the real part w and the imaginary part $v = (x, y, z)$ representing

$$q = w + xi + yj + zk. \tag{4}$$

From this, the relationship for the conversion from the carrier coordinate system to the navigation coordinate system can be expressed as

$$\begin{bmatrix} x_n \\ y_n \\ x_n \end{bmatrix} = \begin{pmatrix} w^2 + x^2 - y^2 - z^2 & 2(xy - wz) & 2(xz + wy) \\ 2(xy + wz) & w^2 - x^2 + y^2 - z^2 & 2(yz - wx) \\ 2(xz - wy) & 2(yz + wx) & w^2 - x^2 - y^2 + z^2 \end{pmatrix} \begin{bmatrix} x_b \\ y_b \\ z_b \end{bmatrix}. \tag{5}$$

As a result, the transformation matrix C_b^n for the conversion from the carrier coordinate system (B-frame) to the navigation coordinate system (N-frame) in 3D space is obtained as

$$C_b^n = \begin{pmatrix} w^2 + x^2 - y^2 - z^2 & 2(xy - wz) & 2(xz + wy) \\ 2(xy + wz) & w^2 - x^2 + y^2 - z^2 & 2(yz - wx) \\ 2(xz - wy) & 2(yz + wx) & w^2 - x^2 - y^2 + z^2 \end{pmatrix}. \tag{6}$$

In quaternion applications, to ensure stability and accuracy in computations, it is essential to normalize quaternions. Normalized quaternions exhibit improved numerical stability and computational efficiency. Therefore, in quaternion calculations, normalization is a critical step. Utilizing quaternions for the transformation from the navigation coordinate system to the carrier coordinate system offers several advantages. It not only helps avoid issues such as gimbal lock and abrupt changes in heading angles but also simplifies and speeds up calculations, making it suitable for real-time attitude determination and navigation applications. Quaternion rotation angles are determined by the real component, denoted as 'w'. Normalization involves dividing the quaternion by its magnitude, resulting in a unit quaternion with a magnitude of 1. The purpose of normalization is to separate the rotation angle and rotation axis represented by the quaternion, facilitating subsequent calculations. Normalized quaternions possess uniqueness, meaning that any nonzero quaternion can be uniquely represented as a product of a unit quaternion and a rotation angle. This uniqueness helps prevent uncertainties and errors in calculations.

Since the inverse of a quaternion is its conjugate divided by the square of the modulus length, the inverse of a quaternion is its conjugate quaternion when the modulus length is 1 after normalization, and the magnitude of the quaternion when it is not normalized is given by

$$\|q\| = \sqrt{w_2 + x_2 + y_2 + z_2}, \tag{7}$$

normalized into

$$\hat{q} = \frac{q}{\|q\|}. \tag{8}$$

3.2   Gait analysis

Gait analysis is the quantitative analysis and recognition of the human walking process, including parameters such as stride length, step width, step frequency, and gait cycle, extracted from a pedestrian's gait. It plays a crucial role in strap-down inertial pedestrian navigation. Gait features refer to the quantifiable parameters extracted from a person's gait, which include stride length, step width, step frequency, gait cycle, and more. Analyzing and recognizing a pedestrian's gait allow for pedestrian identification, posture estimation, and behavior analysis.

This, in turn, improves position estimation and navigation accuracy while enhancing the robustness of the navigation system.

The process of walking can be viewed as a cyclic motion of alternating footfalls and lifts. A complete gait is typically divided into four phases: footfall, stance, post-swing, and pre-swing, as illustrated in Fig. 3. To simplify the full gait into the stance and swing phases, the swing phase represents the moment when the pedestrian's feet are in motion, whereas the stance phase represents the time when the pedestrian's feet are in full contact with the ground. Theoretically, during the stance phase, the angular velocity and horizontal acceleration values are zero, and the vertical acceleration value equals the gravitational constant.

An essential prerequisite for pedestrian navigation is the accurate identification of the stance phase. Signal detection is carried out by distinguishing changes in the acceleration and angular velocity of the inertial sensors. Typically, two conditions must be met: (1) angular velocity condition: $\omega_b^n = 0$ and (2) acceleration condition: $\alpha_b^n = g$. These conditions determine whether the stance phase is in effect. When the stance phase occurs, the detected signal is set to 1, and during the swing phase, the detected signal is set to 0. Traditional single-threshold gait detection algorithms primarily include acceleration variance detection, acceleration amplitude detection, angular rate energy detection, and GLRT. In some specific movements, it can be challenging to achieve accurate gait detection through a single acceleration or angular velocity detection method. The use of the GLRT algorithm can be a viable choice.

3.3 Navigation update

The choice of the "East-North-Up" geodetic coordinate system as the navigation reference coordinate system for the inertial navigation system and its specific force equation is

$$\dot{v}^n = C_b^n f^b - (2\omega_{ie}^n + \omega_{en}^n) \times v^n - g^n. \tag{9}$$

In the equation provided, where f^b represents the specific force measured by the accelerometer, $2\omega_{ie}^n \times v^n$ denotes the Coriolis acceleration generated by the motion of the carrier and Earth's rottion, $\omega_{en}^n \times v^n$ represents the centripetal acceleration due to motion, and g^n signifies the three-

| Landing condition | Standing posture | Back swing state | Front swing state |
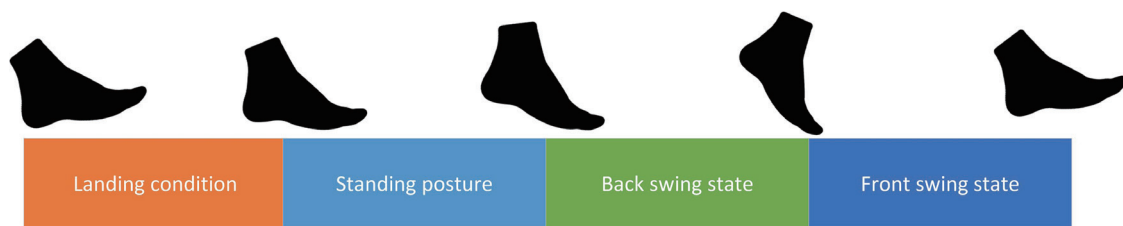
Fig. 3.　(Color online) Gait distribution.

axis components of the gravity acceleration in the navigation coordinate system. To obtain velocity information, the integration of the specific force is performed after removing the detrimental accelerations $2\omega_{ie}^{n} \times v^{n} + \omega_{en}^{n} \times v^{n} + g^{n}$. Following this, the following equation directly yields the formula for velocity updates:

$$v_k^n = v_{k-1}^n + (\frac{C_{b_k}^n f_k^b + C_b^{k-1} f_{k-1}^b}{2} - g^n)\Delta t, \tag{10}$$

where Δt represents the system sampling period, and the position equation can be derived from the equation as

$$\dot{P}^n = v^n. \tag{11}$$

The expression for a position update is

$$P_k^n = P_{k-1}^n + \frac{v_{k-1}^n + v_k^n}{2}\Delta t. \tag{12}$$

Position solving is based on the relative displacement of the pedestrian, and therefore, it is necessary to establish an initial starting position as a prerequisite before initiating navigation. This initial position serves as a reference point for the experiment.

4. Zero Velocity Detection

Zero velocity detection is the process of analyzing pedestrian gait data to determine whether the pedestrian is in a stationary state (zero velocity). The detection principle is based on changes in gait features and motion patterns when a pedestrian is stationary. When a pedestrian is at rest, the gait features and motion patterns exhibit notable changes. The detection process involves analyzing and processing pedestrian gait data to determine if the pedestrian is stationary. Most algorithms for detecting zero velocity intervals in pedestrian gait are based on the comparison of the modulus, variance, and amplitude of the output parameters of the IMU with predefined thresholds. This allows the determination of zero velocity points within the gait. However, this type of algorithm has two main limitations: it is affected by cumulative errors from the IMU, and it can easily lead to the misjudgment of zero velocity intervals due to the brief contact time of the feet with the ground during walking, increasing errors in pedestrian speed and position.

In this study, we employ the GLRT algorithm to detect zero velocity moments during pedestrian walking. If the value of the swing state is denoted as H_0 and the value of the stance state is denoted as H_1, the algorithm models the specific force and angular velocity. Under H_0 (swing state), it is challenging to establish a model for the signal $s_k(\theta)$ that reflects different gait patterns. When in H_1 (stationary state), two conditions are satisfied:

(1) When in a stationary state, the specific force measured by the accelerometer contains only the gravitational acceleration component perpendicular to the ground.

(2) When in a stationary state, the attitude of the IMU remains constant.

These conditions can be expressed as

$$
\begin{aligned}
H_0 &: \exists k \in \Omega_n \ \text{ s.t. } \ s_k^a \neq g u_n \ \text{ or } \ s_k^w(\theta) \neq 0, \\
H_1 &: \exists k \in \Omega_n \ \text{ then } \ s_k^a = g u_n \ \text{ and } \ s_k^w(\theta) = 0.
\end{aligned} \tag{13}
$$

In the equation, θ represents the positional parameter of the output signal $u_n \in \Omega_u$ $\Omega u = \left\{ u \in R^3 : \|u\| = 1 \right\}$. "$g$" represents the gravitational component value at the current location. When a pedestrian is in H_0 (swing state), the signal $s_k(\theta)$ is entirely unknown. When in H_1 (stationary state), the direction of the specific force is unknown, and the unknown parameters are

$$
\begin{aligned}
H_0 &: \theta \equiv \{s_k\}_{k=n}^{n+N-1}, \\
H_1 &: \theta \equiv u_n.
\end{aligned} \tag{14}
$$

Performing maximum likelihood estimation on the unknown parameters leads to the determination of H_1 (stationary state). Combined with Eq. (14), the following formula is obtained:

$$
L_G(z_n) = \frac{p(z_n; \hat{\theta}^1, H^1)}{p(z_n; \hat{\theta}^0, H^0)} > \gamma, \tag{15}
$$

where $\hat{\theta}$ represents the maximum likelihood estimate of the unknown parameters under the assumption of H_1 (stationary state), and $\hat{\theta}$ is the maximum likelihood estimate of the unknown parameters under the assumption of H_0 (motion state). Assuming H_1 (stationary state), only the specific force direction is unknown, i.e., $\theta = u_n$, and the maximum likelihood value of the unknown parameters is obtained from the following formula:

$$
p(z_n; u_n, H_1) = \frac{1}{(2\pi\sigma_a^2)^{3N/2}} \left| -\frac{1}{2\sigma_a^2} \sum_{k \in \Omega_n} \left\| y_k^a - g u_n \right\|^2 \right| \times \frac{1}{(2\pi\sigma_\omega^2)^{3N/2}} \left| -\frac{1}{2\sigma_\omega^2} \sum_{k \in \Omega_n} \left\| y_k^\omega \right\|^2 \right|. \tag{16}
$$

As $u_n \in \Omega$, it follows that

$$\hat{u}_n = \arg\max_{u \in \Omega_u}(p(z_n;u,H_1)) = \arg\min_{u \in \Omega_u}\left(\sum_{k \in \Omega_u}\left\|y_k^a - gu\right\|^2\right)$$

$$= \arg\max_{u \in \Omega_u}\left(\left(\overline{y}_k^a\right)^T u\right) = \frac{\overline{y}_k^a}{\left\|\overline{y}_k^a\right\|}. \tag{17}$$

In the equation,

$$\overline{y}_n^a = \frac{1}{N}\sum_{k \in \Omega_n} y_k^a. \tag{18}$$

Substituting $\hat{u}_n$ into Eq. (16), we obtain

$$p(z_n;\hat{\theta}^1,H_1) = p(z_n;\hat{u}_n,H_1). \tag{19}$$

That is,

$$L_G(z_n) = \left|-\frac{1}{2\sigma_a^2}\sum_{k \in \Omega_k}\left\|y_k^a - g\frac{\overline{y}_n^a}{\left\|\overline{y}_n^a\right\|}\right\|^2 \cdot -\frac{1}{2\sigma_\omega^2}\sum_{k \in \Omega_k}\left\|y_k^\omega\right\|^2\right| > \gamma. \tag{20}$$

After simplification, the GLRT pedestrian zero velocity detection algorithm is

$$T(z_n) = -\frac{2}{N}\ln L_G(z_n), \tag{21}$$

$$T(z_n) = \frac{1}{N}\sum_{k \in \Omega_k}\left(\frac{1}{\sigma_a^2}\left\|y_k^a - g\frac{\overline{y}_n^a}{\left\|\overline{y}_n^a\right\|}\right\|^2 + \frac{1}{\sigma_\omega^2}\left\|y_k^\omega\right\|^2\right) < \gamma'. \tag{22}$$

Including $\gamma' = -\left(\frac{2}{N}\right)\ln\gamma$, the zero velocity detection determination formula is Eq. (22).

5.   Kalman Filtering

Kalman filtering is a recursive filtering algorithm based on a state-space model. It typically involves the weighted fusion of the system's state estimate and measurement data to obtain the optimal state estimation results. In the context of SINSes, Kalman filtering is used to perform the real-time estimation and correction of a pedestrian's position and orientation by fusing sensor measurement data and the system model.

The Kalman filtering algorithm is employed to compensate for bias errors. Initially, the Kalman filtering state vector is expanded from 9 dimensions to 15 dimensions, where X_k represents the state equation. This 15-dimensional state vector includes the estimation of the three-dimensional position s_n, the three-dimensional velocity v_n, the three-dimensional attitude angle θ_n, the three-dimensional accelerometer zero bias values ε_n, and the three-dimensional gyroscope zero bias values α_n.

$$X_k = \begin{bmatrix} s_n^T & V_n^T & \theta_n^T & \varepsilon_n^T & \alpha_n^T \end{bmatrix} \tag{23}$$

By calculations, the accelerometer zero bias values ε_n and the gyroscope zero bias values α_n can be determined. These values can be used to correct the differences in acceleration and angular velocity at the next time step, effectively eliminating zero bias errors.

The Kalman filtering model is

$$\begin{cases} \dot{x} = F_c x + G_c u, \\ z = Hx + R \end{cases} \tag{24}$$

The state transition matrix F_c and the process noise gain matrix G_c are

$$F_c = \begin{pmatrix} 0 & I & 0 & 0 & 0 \\ 0 & 0 & St & Rb2t & 0 \\ 0 & 0 & 0 & 0 & -Rb2t \\ 0 & 0 & 0 & B_1 & 0 \\ 0 & 0 & 0 & 0 & B_2 \end{pmatrix}, \tag{25}$$

$$G_k = \begin{pmatrix} 0 & 0 & 0 \\ Rb2t & 0 & 0 \\ 0 & -Rb2t & 0 \\ 0 & 0 & I \\ 0 & 0 & 0 \\ 0 & 0 & 0 \\ 0 & 0 & 0 \end{pmatrix}, \tag{26}$$

where St is the skew-symmetric matrix of a specific force vector, and its matrix elements are created on the basis of accelerometer values in the navigation coordinate system. B_1 and B_2 are the bias correlation coefficients for the accelerometer and gyroscope, respectively.

$$St = \begin{pmatrix} 0 & -a_{zk} & a_{yk} \\ a_{zk} & 0 & -a_{xk} \\ -a_{yk} & a_{xk} & 0 \end{pmatrix} \tag{27}$$

The Kalman filtering model is

$$\begin{cases} X_k = Fx_{k-1} + Gu_{k-1}, \\ Z_k = Hx_k + R \end{cases} \tag{28}$$

6. Sliding Window

The sliding window algorithm can be used for real-time correction in pedestrian navigation by analyzing and optimizing measurement data within a sliding window in a continuous time or spatial sequence. It allows for the continuous estimation and correction of the pedestrian navigation state, making it suitable for pedestrian navigation algorithms that require real-time responses and updates. In inertial pedestrian navigation, position and velocity information can be considered as a time sequence, and subsequences that meet specific conditions can be found and corrected to gradually update the current state estimation. A sliding window is defined with the sliding interval $T_k \in [T_{max}, T_{min}]$, where T_k represents the width of the sliding window at time k, T_{max} is the upper limit of the width, and T_{min} is the lower limit of the width. Depending on the actual situation, the width of the window slides within this range, allowing for a rapid response to changes in measurement noise. When measurement noise is in a steady state, it is advisable to choose a larger T value to effectively improve the precision of measurement noise correction. When measurement noise undergoes periodic changes, smaller T values should be chosen to enhance tracking sensitivity.

Pedestrian orientation is described by three Euler angles (pitch, roll, and yaw). The inertial navigation system can be represented as a 3D vector:

$$x_k = [\phi_k, \theta_k, \psi_k]^T. \tag{29}$$

Following the sliding window principle, the current state estimate is gradually corrected using historical data, and the state values for the pedestrian over the most recent N time steps are stored in the matrix X_k:

$$X_k = [x_{k-N+1}, \ldots, x_{k-1}, x_k]. \tag{30}$$

The least squares method is used to estimate and optimize the state values within the window. The goal of the least squares optimization is to minimize the sum of the squares of the observation residuals, which means minimizing the differences between the measured and predicted values. Through least squares optimization, based on the historical data observed

within the window and the prediction model, the optimal estimate of the pedestrian's walking path is obtained. This can be achieved by solving a system of equations to obtain the estimated state vector.

$$X_k = A_k x_k + v_k \tag{31}$$

Here, A_k is a $3N \times 3$ coefficient matrix and v_k is a $3N \times 1$ noise term. Each row of the coefficient matrix is constructed from the historical data's attitude information. The noise term represents measurement errors and model uncertainties. The goal is to minimize the estimation error by solving the following least squares formula:

$$\hat{x}_k = \arg\min_{x_k} \left\| X_k - A_k x_k \right\|_2^2. \tag{32}$$

The closed-form solution for this formula is

$$\hat{x}_k = (A_k^T A_k)^{-1} - A_k^T X_k, \tag{33}$$

which is used to estimate the equivalent current state $\hat{x}_k$ at the current time step. The sliding window width, which is determined by the upper limit T_{max} for tracking accuracy and the lower limit T_{min} for tracking sensitivity, is updated on the basis of historical data and the current state estimate. A larger T_{max} is preferred to ensure higher tracking accuracy, but a window width of 200 already guarantees relatively high tracking accuracy. Further increasing the window width does not significantly improve tracking accuracy. To balance tracking accuracy and computational efficiency, a window length in the range of $200 \leq T_{max} \leq 300$ is recommended. As for the lower limit T_{min}, it should be as small as possible to maintain tracking sensitivity. An excessively small window width may result in reduced tracking sensitivity. A window length in the range of $40 \leq T_{min} \leq 60$ is considered suitable.

The sliding window algorithm for navigation correction offers several advantages, including real-time capability, flexible window control, and smoothness. By leveraging statistical information from historical data, it allows for state estimation and correction. It takes into account trends in historical data and the dynamic nature of the system, leading to improved navigation accuracy and stability. Additionally, the algorithm can be adjusted flexibly on the basis of specific application scenarios and requirements, allowing the selection of an appropriate window size and optimization method to meet practical navigation needs.

7.   Experiments and Analysis

7.1   Experimental configuration

The inertial sensor core features a high-performance Cortex-M4 processor with a clock frequency of up to 168 MHz, providing a balance between low power consumption and high

performance. This enables rapid real-time motion and attitude calculations. The module includes an integrated voltage stabilizing circuit, supporting operating voltages from 3.3 to 5 V, with pin-level compatibility for 3.3 V/5 V embedded systems. It also supports stable Bluetooth Low Energy (BLE) 5.0 wireless transmission, with a transmission range of up to 50 m. The performance parameters of the inertial sensor are detailed in Tables 1 and 2.

Figure 4(a) shows the experimental environment and IMU device fixed to the foot, and Fig. 4(b) shows the hardware relationship structure.

## 7.2	Pedestrian localization trajectory

To validate the practical performance of this solution, two experiments were conducted: circular route testing indoors and square route testing outdoors, both in a controlled environment.

Table 1
Detailed indicators of acceleration parameters.

Acceleration parameters	Conditions	Typical values
Range		±16 g
Resolution	±16 g	0.0005 (g/LSB)
RMS noise	Bandwidth = 100 Hz	0.75–1 mg-rms
Static zero bias	Horizontally placed	±20–40 mg
Temperature drift	−40–+85 ℃	±0.15 mg/℃
Bandwidth		5–256 Hz

Table 2
Detailed indicators of gyroscope parameters.

Gyroscope parameters	Conditions	Typical values
Range		±2000°/s
Resolution	±2000°/s	0.061(°/s)(LSB)
RMS noise	Bandwidth = 100Hz	0.028–0.07(°/s)-rms
Static zero bias	Horizontally placed	±0.5–1°/s
Temperature drift	−40–+85 ℃	±0.005–0.015(°/s)/℃
Bandwidth		5–256 Hz

Inertial Sensor				Bluetooth				Laptop Computer

(a)											(b)
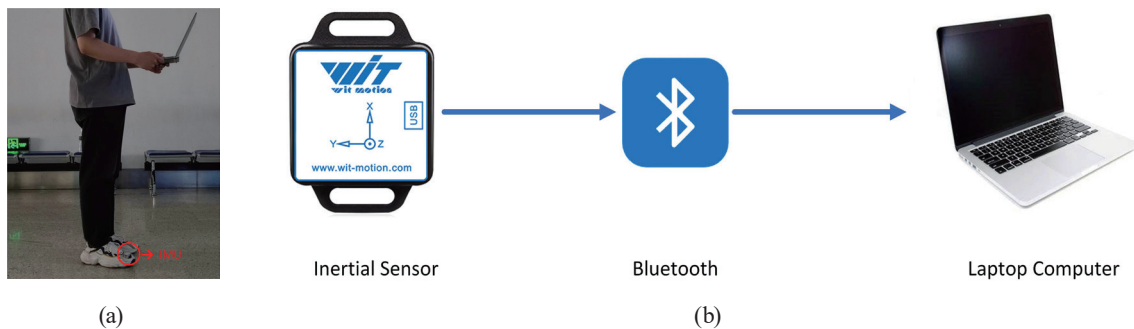
Fig. 4.	(Color online) (a) Experimental environment and (b) hardware relationship structure.

7.2.1   Circular-square closed-loop trajectory test

Inertial sensors were strapped to the tops of the feet for walking experiments. To test the localization performance of the pedestrian navigation algorithm in a flat ground environment, the experimenter walks in a circle at a slow pace, a normal pace, and a fast pace, and the endpoint localization error can be measured by the distance between the starting points since the endpoints and the starting points in the walking route are the same. The circular trajectory path is a circular flowerbed of 30 m diameter.

Zero Velocity Update (ZUPT), which represents zero-update technology, is a calibration method commonly used in inertial navigation systems. An inertial navigation system is a system that utilizes inertial sensors, such as accelerometers and gyroscopes, to track the position, direction, and speed of a vehicle, aircraft, or other moving objects. However, these sensors usually accumulate errors that result in the inaccurate output of the navigation system. ZUPT is one of the techniques used to calibrate these errors. In the ZUPT technique, the drift error of the gyroscope is eliminated by calibrating the system at a moment when the velocity is known to be zero. In this way, when a moving object is at rest, by detecting the output of the accelerometer, the zero-rate moments can be recognized, and this information can then be used to calibrate the gyroscope. The basic principle of ZUPT is that when an object is at rest, it has zero velocity, and thus the angular velocity of the gyroscope output should be zero. Therefore, when the angular velocity of the gyroscope output is detected to be close to zero, it can be considered a ZUPT moment. At such moment, the output of the accelerometer can be utilized to calibrate the gyroscope. The goal of the ZUPT technique is to eliminate or minimize these errors by calibrating at moments when the velocity of the object is known to be zero. Its basic principle is to utilize the information from the outputs of the accelerometer and gyroscope. When the object is at rest, the output of the accelerometer should contain only the gravitational acceleration component, while the output of the gyroscope should be zero. Therefore, when the angular velocity of the gyroscope output is detected to be close to zero, it can be considered as a ZUPT moment.

Figure 5 shows the results of gait detection in the circular trajectory experiment. The horizontal axis represents time, and the vertical axes with values 0 and 1 indicate the stance and swing phases, respectively. In the curve of ZUPT detection versus time, the horizontal coordinate is the pedestrian walking time in seconds, the vertical coordinate is the ZUPT detection value, and the value 0 means that the pedestrian is in H_0 (swinging state) and the value 1 means that the pedestrian is in H_1 (stationary state). The results showed that the pedestrian zero-speed point judgment is normal under the GLRT algorithm, which proves that the algorithm can be effectively applied to the zero-speed detection. The results showed that the judgment of the pedestrian zero speed point is normal under the GLRT algorithm, which proves that the algorithm can be effectively applied in zero speed detection.

Figure 6 shows the actual route of the pedestrian walking one lap in reverse. In Fig. 6, the red line represents the pedestrian true trajectory and the blue line represents the ZUPT + sliding window algorithmic solution trajectories. The endpoint positioning error is calculated using the formula $\delta_{location} = d_{terminus}/D_{total\_distance}$. In the experiment, we used three different walking
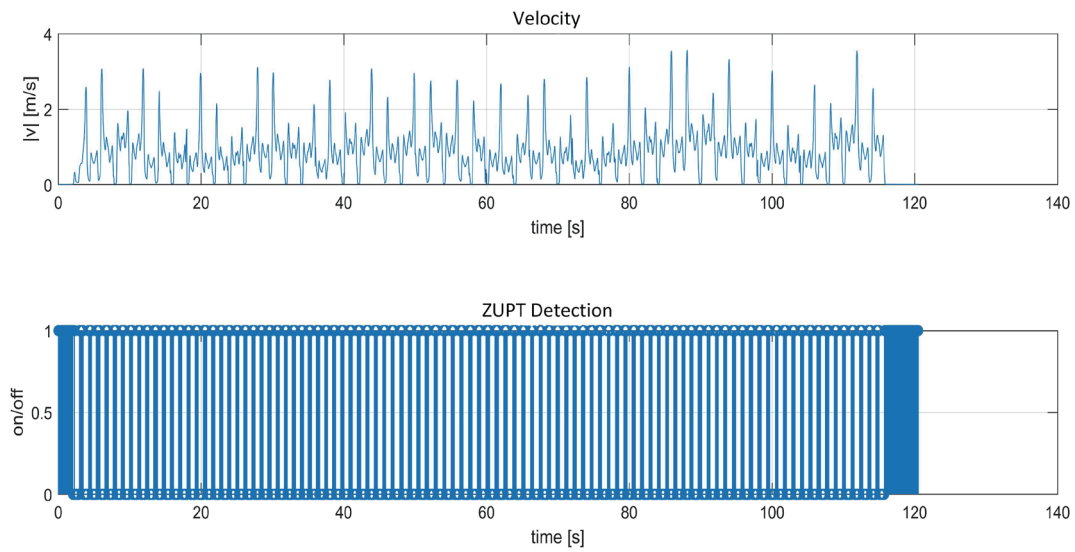
Fig. 5.   (Color online) Gait zero velocity detection results.
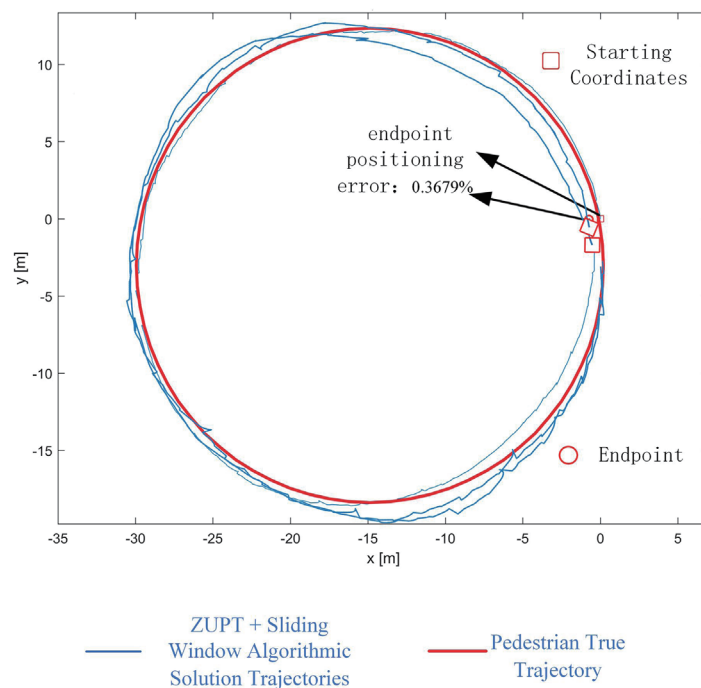
Fig. 6.   (Color online) Circular Path ZUPT + Sliding Window.

speeds. The calculated localization errors are 0.3679% for slow walking, 0.4125% for normal walking, and 0.4764% for fast walking. In Fig. 7, the red line represents the pedestrian true trajectory. The blue line represents the simulated path using ZUPT. The calculated localization errors are 4.72744% for slow walking, 5.6783% for normal walking, and 6.7894% for fast walking, which are higher than the positioning error under the ZUPT+Sliding Window fusion algorithm, as shown in Fig. 6.
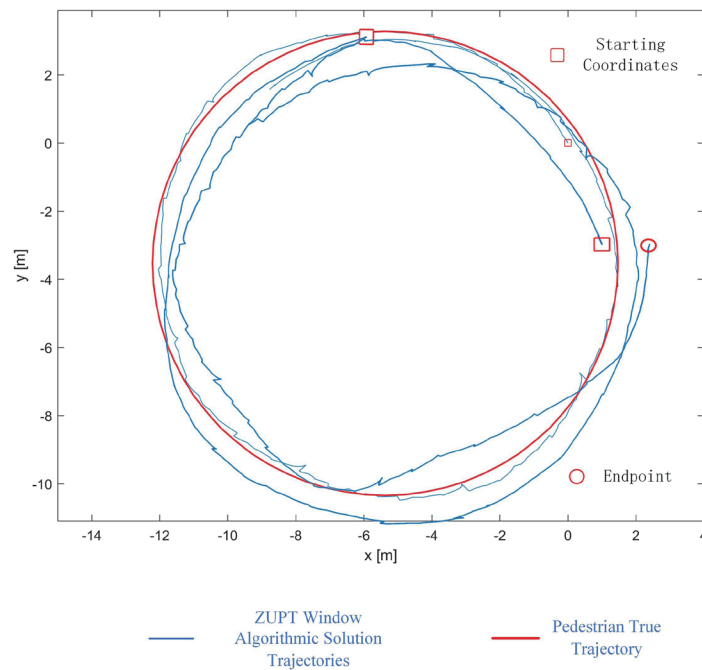
Fig. 7.   (Color online) Circular Path-ZUPT.

The comparison of the two figures shows that the three circles of trajectories applying our proposed algorithm basically overlap, and the error with the circular true route is extremely small, which considerably improves the pedestrian navigation accuracy. This result indicates that the ZUPT+Sliding Window fusion algorithm can effectively correct navigation errors.

The rectangular path is around a 13.00 m × 11.00 m square flowerbed with four 90° right-angle turns. The experimental results are shown in Fig. 8, which shows the pedestrian true trajectory as the red line and ZUPT + Sliding Window algorithmic solution trajectories as the blue line. By using the endpoint location error calculation formula $\delta_{location} = d_{terminu}/D_{total\_distance}$, the calculated localization errors are 1.564% for slow walking, 1.634% for normal walking, and 1.967% for fast walking.

In Fig. 9, the red line represents the pedestrian true trajectory and the blue line represents the ZUPT algorithmic solution trajectories. The calculated localization errors are 17.8089% for slow walking, 18.7809% for normal walking, and 18.9876% for fast walking. These errors are greater than those in Fig. 8, which represents the ZUPT + Sliding Window algorithm's simulated path. These results demonstrate that the ZUPT + Sliding Window fusion algorithm effectively corrects navigation errors.

Through these two experiments, it is evident that the navigation system in this study exhibits high precision and effectively addresses common issues such as accumulated drift errors and low directional estimation accuracy in navigation systems. Table 3 provides a comparison of the experimental results under different methods.
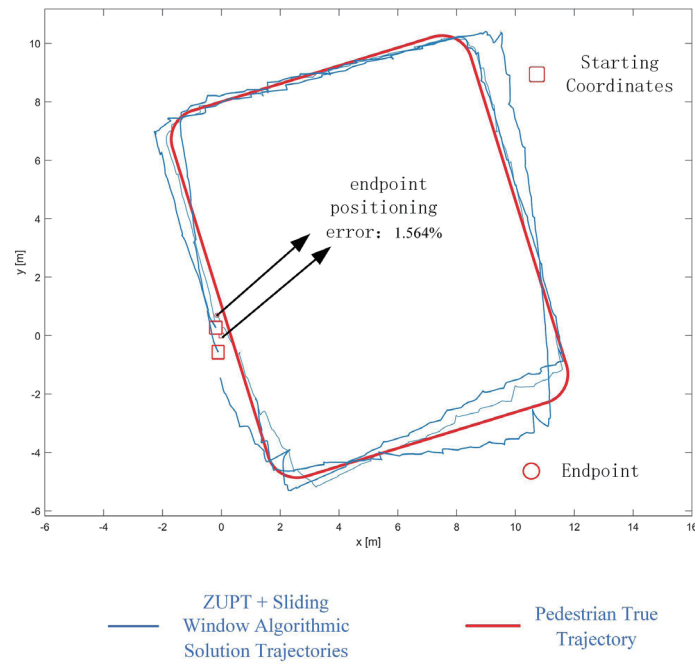
Fig. 8.   (Color online) Square Path-ZUPT + Sliding Window.
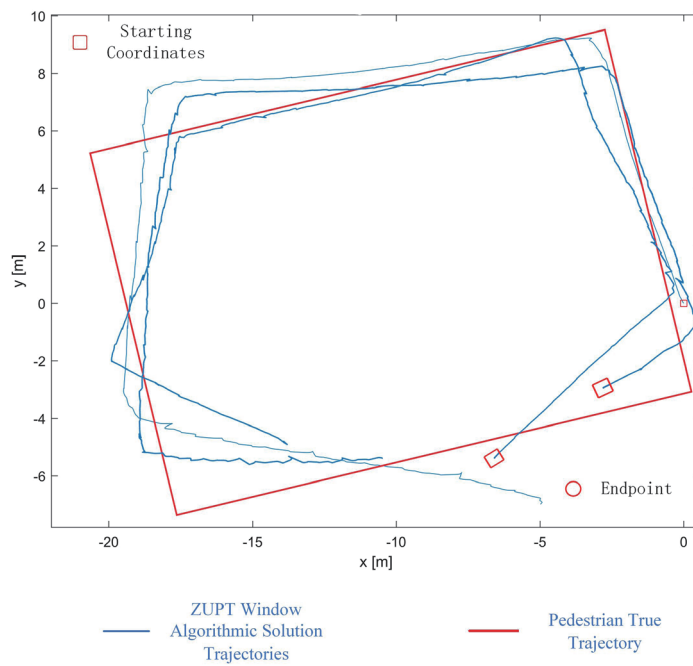
Fig. 9.   (Color online) Square Path-ZUPT.

Table 3
Comparison results.

Algorithm	Total_distance/m		Walking speed		Positioning error/%	
	Circular trajectory	Rectangular trajectory	Circular trajectory	Rectangular trajectory	Circular trajectory	Rectangular trajectory
ZUPT + Sliding	188.2	48	Slow speed	Slow speed	0.3679	1.564
	188.2	48	Normal speed	Normal speed	0.4125	1.634
	188.2	48	Fast walking	Fast walking	0.4764	1.967
ZUPT	188.2	48	Slow speed	Slow speed	4.72744	17.8089
	188.2	48	Normal speed	Normal speed	5.6783	18.7809
	188.2	48	Fast walking	Fast walking	6.7894	18.9876
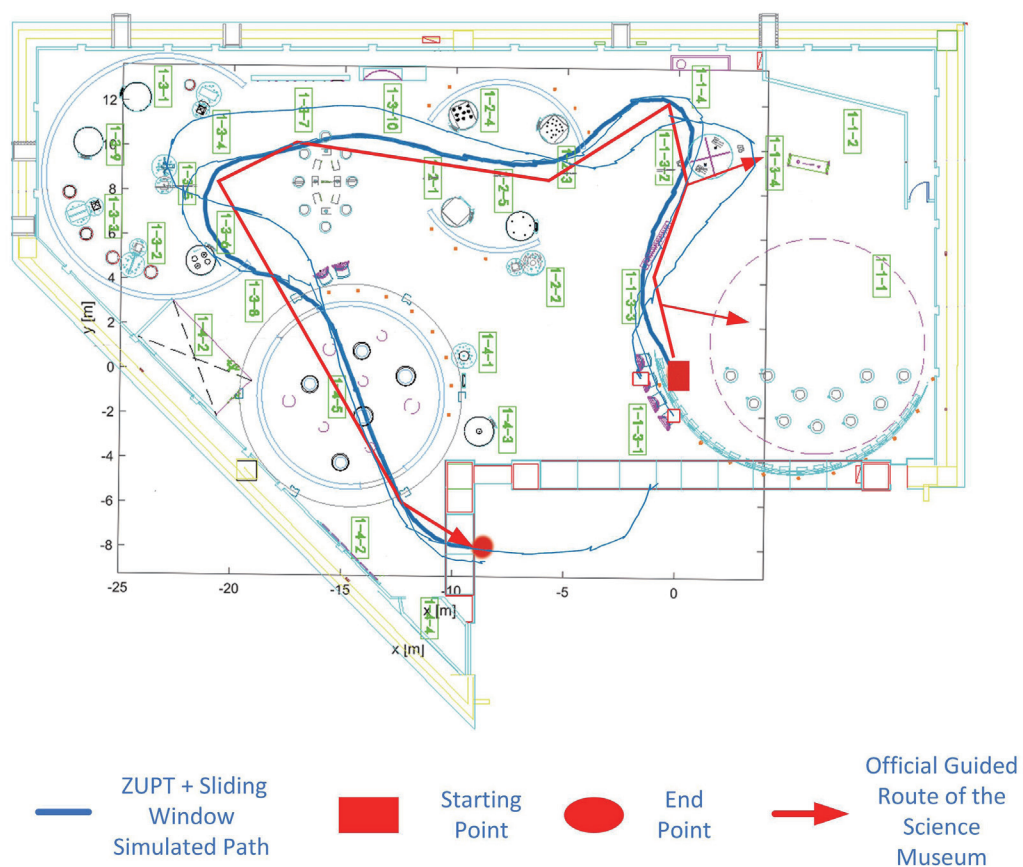
Fig. 10.　(Color online) Science museum route.

7.2.2　Complex environment testing

The testing location chosen for this experiment is the First Hall of the China Science and Technology Museum, specifically in the "Wonderful Light" exhibition hall. The experimental results are shown in Fig. 10.

Figure 10 shows the CAD modeling diagram of the China Optics Science and Technology Museum - First Exhibition Hall Wonderful Light Showroom. The red path is the official

navigation path, the blue path is the algorithm-solved path, the pedestrians are tested using three walking modes (slow, normal speed, and fast), and the trajectory is found to be basically consistent after comparison. The complex walking experiments in the showroom further proved the improvement of the positioning accuracy of the system by the fusion ZUPT+Sliding Window algorithm.

8.   Conclusion

An indoor pedestrian navigation algorithm based on MEMS inertial sensors has been developed, incorporating a ZUPT mechanism designed to exploit the characteristics of acceleration and angular velocity data from these sensors. This algorithm utilizes the GLRT for zero velocity detection. Additionally, it employs a sliding window algorithm in conjunction with gait classification methods, which are combined with Kalman filtering to refine and track the pedestrian's trajectory. Experimental results demonstrate that in both indoor and outdoor environments where GPS signals are unavailable, navigation errors remain below 2%. This algorithm effectively meets pedestrian navigation needs and can provide long-term, accurate tracking and positioning.

Acknowledgments

References

1   Y. Zhang: IEEE Access **7** (2019) 61296. https://doi.org/10.1109/ACCESS.2019.2911025
2   K.-Y. Qiu, H. Huang, W. Li, and D.-A. Luo: Sens. Mater. **10** (2019) 3303. https://doi.org/10.18494/SAM.2019.2460
3   V. Magnago, L. Palopoli, A. Buffi, B. Tellini, A. Motroni, P. Nepa, D. Macii, and D. Fontanelli: IEEE Trans. Instrum. Meas. **69** (2020) 2408. https://doi.org/10.1109/TIM.2019.2960900
4   S. Youm and K.-S. Shin: Sens. Mater. **6** (2021) 2083. https://doi.org/10.18494/SAM.2021.3303
5   O. Bebek, M. A. Suster, S. Rajgopal, M. J. Fu, X. Huang, M. C. Cavusoglu, D. J. Young, M. Mehregany, A. J. van den Bogert, and C. H. Mastrangelo: IEEE Access **1** (2010) 1052. https://api.semanticscholar.org/CorpusID:4439476
6   X. Tian, J. Chen, Y. Han, J. Shang, and N. Li: Sensors **16** (2016) 1578. https://doi.org/10.3390/s16101578
7   W. Shi, Y. Wang, and Y. Wu: Sensors **17** (2017) 427. https://doi.org/10.3390/s17020427
8   J. Yang, Y. Liu, J. Zhang, Y. Guan, and Z. Shao: Int. J. Adv. Rob. Syst. **21** (2024) 5. https://doi.org/10.1177/17298806241292893
9   M. Bamdad, H.-P. Hutter, and A. Darvishy: Sensors. **24** (2024) 8164. https://doi.org/10.3390/S24248164
10 Q. Wang, M. Fu, J. Wang, L. Sun, R. Huang, X. Li, Z. Jiang, Y. Huang, and C. Jiang: Def. Technol. **33** (2024) 573. https://doi.org/10.1016/J.DT.2023.03.001
11 X. Wang, J. Li, G. Xu, and X. Wang: Sensors. **24** (2024) 3. https://doi.org/10.3390/S24030838
12 F. Huang, M. Gao, Q. Liu, F. Tang, and Y. Wu: Meas. Sci. Technol. **34** (2023) 10. https://doi.org/10.1088/1361-6501/ACE377
13 L. An, X. Pan, T. Li, and M. Wang: J. Sens. **2022** (2022) 1. https://doi.org/10.1155/2022/1311221
14 Y. Wang, C.-S. Jao, and A. M. Shkel: Gyroscopy and Navigation **12** (2021) 1. https://doi.org/10.1134/S2075108721010119
15 X. Wu, L. Zhao, S. Guo, and L. Zhang: J. Phys. Conf. Ser. **1903** (2021) 1. https://doi.org/10.1088/1742-6596/1903/1/012043

16   W. Li, Z. Xiong, Y. Ding, Z. Cao, and Z. Wang: IEEE Access **9** (2021) 42059. https://doi.org/10.1109/ACCESS.2021.3065666
17   M. Uradzinski and H. Guo: J. Sens. Sens. Syst. **9** (2020) 7. https://doi.org/10.5194/jsss-9-7-2020

About the Authors

Boqi Wu is a Doctor of Engineering and serves as the academic backbone of the Key Laboratory of Comprehensive Energy Conservation in Cold Region Buildings under the Ministry of Education. She also holds the position of master's supervisor and is recognized as a Class D talent in Jilin Province.

Chenyang Cao graduated from Suihua University in 2016. He is currently studying for a master's degree at Jilin Jianzhu University. His current research field is MEMs-based pedestrian inertial navigation. (2422399297@qq.com)

Yang Zhao graduated from Northeast Normal University. His research interests include the power management of storage batteries in ocean tidal current power generation systems, model parameter identification, and state estimation based on the data-driven equivalent circuit model estimation method.

Yaodan Chi is currently the dean of the College of Electrical and Computer Science of Jilin Jianzhu University, the director of the Key Laboratory of Building Comprehensive Energy Conservation in Cold Areas of the Ministry of Education, and the director of the "Jilin Province Cold Area Building Energy Conservation Science and Technology Innovation Center" of the Provincial Science and Technology Department. (147670107@qq.com)